Oral Qualifier: An Introduction to Electron Polarimetry

Greg Blume

October 2023

1 Introduction

Spin polarized electron beams are produced by photoemission from GaAs photocathodes in dc-high voltage electron guns. They play an essential role for electron accelerators with experiments studying the spin structure of nucleons [1, 2] or the Standard Model [3]. Measuring the beam polarization is therefore also required for these experiments. This is the role of an electron beam polarimeter.

There are only a few techniques that are employed to measure the electron beam polarization. At high energies ($> 1\,\mathrm{GeV}$) the techniques are by Møller (e^-/e^-) [4, 5] and Compton (e^-/γ) [6] scattering. However, at lower energies ($<10\,\mathrm{MeV}$), typically found in a polarized electron injector, these techniques become impractical.

Here, the most common approach is to use Mott-scattering (e^-/Z) [7], where a spin polarized beam scattering rate asymmetry is observed when interacting with the nuclear potential of an atom. These so called Mott-scattering polarimeters can be divided into two types: retarding field ($\mathrm{E} \leq 20\,\mathrm{keV}$) [8] and thin foil ($100\,\mathrm{keV} < \mathrm{E} \leq 10\,\mathrm{MeV}$) [9, 10].

An alternative, although less often used, method at somewhat higher energies ($1\,\mathrm{MeV} < \mathrm{E} \leq 1000\,\mathrm{MeV}$) [11, 12] is by Compton scattering of secondary radiation produced by a polarized electron beam. This so called Compton transmission polarimeter has both benefits and drawbacks to the Mott-scattering approach that will be discussed in detail later.

In this work we introduce the scattering theory that governs the operation of these instruments as well as explain their operational parameters. This will include experimental results obtained at the Upgraded Injector Test Facility (UITF) beamline at Jefferson Lab, where a Mott-scattering and Compton transmission polarimeter were used. Finally, we will conclude with a comparison between the three methods and discuss applications for each.

2 Theory

2.1 Mott-scattering

Mott scattering makes use of electrons scattered elastically off the Coulomb field of a heavy-Z target [7] (ie. gold) given by an integrated cross section [13]

$$\sigma(\theta, \phi) = I(\theta)[1 + S(\theta)\vec{P} \cdot \hat{n}], \tag{1}$$

where the unpolarized (Coulomb-scattering) cross section is

$$I(\theta) = \frac{Z^2 e^4}{4m^2\beta^4 c^4 \sin^2(\theta/2)}[1 - \beta^2 \sin^2(\theta/2)](1 - \beta^2), \tag{2}$$

and $\vec{P}$ is the polarization vector, $\hat{n} = \frac{\vec{k}\times\vec{k'}}{|\vec{k}\times\vec{k'}|}$ is the unit vector determined by the electron momentum before ($\hbar\vec{k}$) and after ($\hbar\vec{k'}$) scattering and is perpendicular to the scattering plane, and $S(\theta)$ is the Sherman Function [14]. The Sherman function can be computed numerically [15, 16] (see Figure 1) as a function of scattering angle and kinetic energy for electrons scattering off a gold atom. Ultimately, the property that makes Mott scattering desirable is the dot product between $\vec{P}$ and $\hat{n}$.

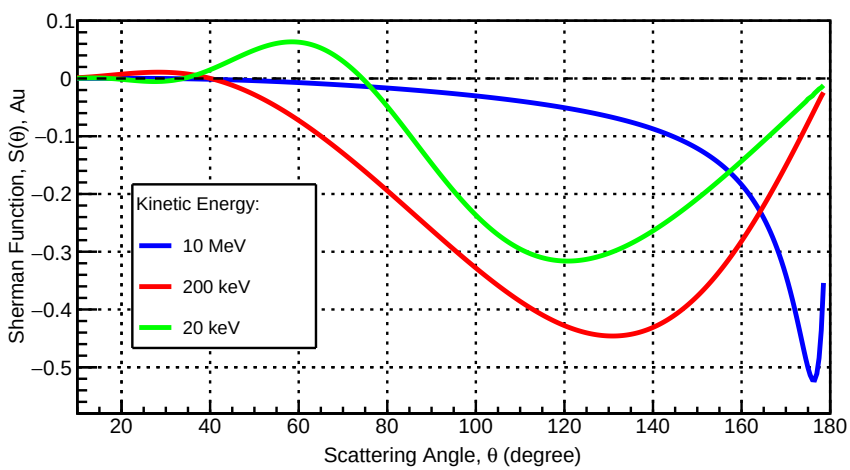

Figure 1: The Sherman function for three kinetic energies similar to those seen at Jefferson Lab as a function of angle. Here, the target was assumed to be gold.

Due to the definition of the unit vector $\hat{n}$ above, the polarization needs to be normal to the scattering plane for the dot product in Eq. 1 to be non-zero.

Assuming the beam is transversely polarized, this property has the advantage that two detectors, given an equal angular displacement from the incident beam direction, will have equal and opposite contribution of the spin dependent scattering rate proportional to $P * S(\theta)$. This is beneficial because the count of electrons scattered into either one of the two detectors will then correspond to either $1 + PS(\theta)$ or $1 - PS(\theta)$.

Experimentally, a counting asymmetry can be observed between the two detectors if the spin polarization was perpendicular to the momentum-detector plane. This asymmetry has the form

$$A = \frac{N_L - N_R}{N_L + N_R}, \tag{3}$$

where N_L and N_R are the number of electrons observed in the beam left and beam right detectors. Now, to a factor of -1, which corresponds to the direction of the polarization vector, $N_L \propto 1 + PS(\theta)$ and $N_R \propto 1 - PS(\theta)$. Thus,

$$A = \frac{1 + PS(\theta) - 1 - PS(\theta)}{1 + PS(\theta) + 1 - PS(\theta)} = \frac{2PS(\theta)}{2} = PS(\theta), \tag{4}$$

where if $S(\theta)$ is known, the beam polarization can be extracted by dividing the experimental asymmetry by the Sherman function. Additionally, the Mott Left-Right asymmetry can be observed using only one detector if the direction of polarization, or helicity, is reversed. The asymmetry then occurs between helicity states as opposed to detectors. The method of observing the experimental asymmetry is what distinguishes the two types of Mott-scattering polarimeters and will be discussed later.

2.2 Compton-scattering

Unlike Mott-scattering polarimetry, Compton transmission polarimetry requires an additional step to extract a polarization measurement. Here, a longitudinally polarized electron beam strikes a radiator producing elliptically polarized bremsstrahlung radiation. These polarized photons are then incident on a polarized target where the photons scatter from the spin-polarized electrons in the target. In this process, the information corresponding to the longitudinal polarization of the initial electron beam is retained in the resulting circular polarization of the bremsstrahlung radiation.

A polarization dependent cross section can be used to describe the interaction between the polarized photons and the polarized target given as

$$\frac{\mathrm{d}^2\sigma}{\mathrm{d}\Omega} = \frac{\mathrm{d}^2\sigma^0}{\mathrm{d}\Omega} \left[1 + P_\mathrm{t} P_\gamma^\mathrm{c} A_\mathrm{C}(\theta)\right], \tag{5}$$

where P_t is the target polarization, P_γ^c is the photon circular polarization, $\mathrm{d}^2\sigma^0/\mathrm{d}\Omega$ is the unpolarized Compton cross section

$$\frac{\mathrm{d}^2\sigma^0}{\mathrm{d}\Omega} = \frac{1}{2}\left(r_0 \frac{\omega}{\omega_0}\right)^2 \left[\frac{\omega_0}{\omega} + \frac{\omega}{\omega_0} - \sin^2(\theta)\right], \tag{6}$$

and

$$A_{\mathrm{C}}(\theta) = \left[\frac{\omega_0}{\omega} - \frac{\omega}{\omega_0}\right]\cos(\theta) \Big/ \left[\frac{\omega_0}{\omega} + \frac{\omega}{\omega_0} - \sin^2(\theta)\right] \tag{7}$$

is the analyzing power of the Compton process. Analogous to Mott-scattering polarimetry, a transmission asymmetry is produced between left circular and right circular polarized photons. Accounting for transmission and absorption within the target [17], the asymmetry can be written

$$A_{\mathrm{T}} = \frac{N^+ - N^-}{N^+ + N^-} = \tanh(-P_{\mathrm{t}} P_{\gamma}^{\mathrm{c}} \mu_1 L) \approx -P_{\mathrm{t}} P_{\gamma}^{\mathrm{c}} \mu_1 L, \tag{8}$$

where $N^{\pm}$ are the number of transmitted photons for each polarization, L is the length of the polarized target, and μ_1 is a polarized Compton absorption coefficient. In order to extend this process to an electron beam, the circular photon polarization can be related to the electron beam polarization via a polarization transfer coefficient $\mathcal{T}$ (that is in principle energy dependent) [18, 19], which, again to a factor of -1, allows the transmission asymmetry to be written as

$$A_{\mathrm{T}} = P_{\mathrm{e}}^{\mathrm{l}} P_{\mathrm{t}}\, \mu_1 \mathcal{T}\, L = P_{\mathrm{e}}^{\mathrm{l}} \mathcal{A}_{\mathrm{eff}}, \tag{9}$$

where $\mathcal{A}_{\mathrm{eff}} = P_{\mathrm{t}}\, \mu_1 \mathcal{T}\, L$ and is an effective analyzing power of the polarimeter. The transmission asymmetry can be represented analytically with the average polarization dependent transmission efficiency as well as the photoelectric and pair creation processes. Together they are used to observe a photon energy deposition following the polarized target [20]. However, these calculations only contribute to a more accurate understanding of $\mathcal{A}_{\mathrm{eff}}$ and are beyond the scope of this report.

This expression is occasionally written $A_{\mathrm{T}} = P_{\mathrm{e}}^{\mathrm{l}} P_{\mathrm{t}} A$ where A is the analyzing power of the polarimeter. However, knowing the target polarization with high precision, less than a few percent, can be difficult because it requires knowing the actual field strength and polarizabilities of the material which vary with temperature and other material properities. Naturally this lends to introducing $\mathcal{A}_{\mathrm{eff}}$ assuming the target is operated consistently during experiment. Similar to Mott polarimetry, if $\mathcal{A}_{\mathrm{eff}}$ is well known, the electron beam polarization can be extracted. Unfortunately, unlike the Sherman function, A and $\mathcal{A}_{\mathrm{eff}}$ are difficult to produce numerically [21, 22, 23]. Instead, $\mathcal{A}_{\mathrm{eff}}$ is typically found experimentally, via a calibration from another polarimeter.

3 Polarimeters

3.1 Retarding Field Mott Polarimeters

In the discussion of the Mott-scattering theory, the math was idealized to assume that all scattering events were elastically scattered electrons. Obviously, real scattering experiments do not have this luxury as electrons often scatter multiple

times, sometimes inelastically. A retarding field Mott polarimeter [8] introduces a repulsive electrostatic field in front of the detectors to filter scattered electrons which have lost energy. This is one approach to isolate elastically scattered electrons.

Retarding field Mott polarimeters [8] begin by producing a longitudinally polarized electron beam with low energy, on the order of 100s of eV. This low energy is beneficial for the purpose of rotating the beam momentum without altering the direction of polarization. Thus, electrostatic lenses are able to deflect to beam incident on a thick heavy-Z target with transverse polarization. Next, once it reaches the scattering chamber the target, attractively biased to high voltage, the electron accelerates towards the target. The electron then scatters from the gold target, resulting in a spin dependent angular distribution. The scattered electrons travel away from the target decelerating due to the same electric field from the target.

Electrons having undergone a perfectly elastic scattering event will reach the edge of the scattering chamber with exactly the initial energy it began with. The detectors are placed along the edge of the chamber with electrostatic grids in front of the them. These grids are repulsively biased with the goal of slowing down, or retarding, the incident electron. Depending on the bias, only quasi-elastic electrons can make it through this retarding field. Polarimeters employing this geometry are referred to as retarding field polarimeters.

In principle, these grids could be bias to just below the initial energy which would only allow perfectly elastic events to be recorded by the detector. However, the rate of such events is so low this is not a practical solution to measuring the scattering asymmetry. Instead, the grid is bias to allow quasi-elastic scatterings to be detected. This bias is then increased to approach the elastic scattering threshold. A linear extrapolation can be applied to produce a result for only elastic scattering.

This asymmetry, normalized to the calculated Sherman function of the target, can be used to extract the polarization of the electron beam. This process is shown in Figure 2.

3.2 Thin Foil Mott Polarimeters

Thin foil Mott polarimeters reduce secondary scattering by removing the number of possible nuclei for scattering by making the targets extremely thin (on the nm scale). Ideally, a single-atom target could be used, but both the physical constraints in constructing such a target as well and the low rate of scattered electrons make this an impractical option. The thin foil technique allows for the connection to a single-atom scattering asymmetry by scattering from foils of different thicknesses and extrapolating to a "zero-thickness" asymmetry. This option is restricted in the retarding field method because swapping targets is not easily accomplished. The extrapolation for a zero-thickness asymmetry is non-linear and takes the form

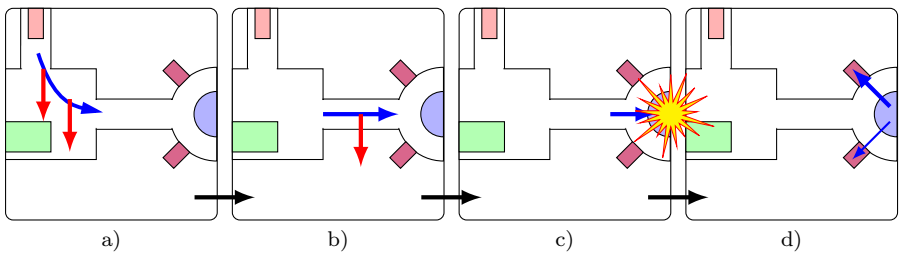

Figure 2: Concept of a retarding field Mott polarimeter. a) A longitudinally polarized electron beam is created at the surface of the photocathode (light-red). The low energy beam direction is deflected (blue arrow) by electrostatic lenses (light-green) while the spin polarization (red) remains in the original orientation. b) The beam polarization is transverse to the momentum and is incident towards the heavy-Z target. c) The electron beam is accelerated towards the biased target and scattering occurs. d) Left-Right detectors observe a count asymmetry (here shown as Top-Bottom for graphics). Retarding field grids isolate elastically scattered events reaching the detectors, allowing for experimental extraction of the asymmetry.

$$A = \frac{A_E(t=0)}{1.0 + \beta t}, \tag{10}$$

where $A_E(t = 0)$ is the zero thickness asymmetry and β characterizes the dependence of the measured asymmetry on target thickness. This form assumes their are no contributions from secondary scattering which is an oversimplification. An increased level of accuracy can be introduced but that is beyond the scope of this work [24].

This zero-thickness asymmetry, along with the Sherman function at the beam energy, can be used to extract the polarization of the electron beam. This process is shown in Figure 3.

3.3 Compton Transmission Polarimeters

The elliptically polarized bremsstrahlung radiation created from the scattering of electrons on a radiator is the first step to measuring polarization using a Compton transmission polarimeter. This radiation is then collimated to reduce the magnitude of photons reaching the polarized target. These photons then scatter off the polarized electrons generating a transmission asymmetry that can be observed in the energy deposit of a photon absorber located after the target.

Unlike Mott polarimetry the rate here is extremely high. Thus, absorbers are often added in front of the photon detector to reduce the count of incident photons. The detector is a scintillating crystal that produces an optical signal corresponding to the number of incident polarized photons. This signal is observed by a photo-multiplier tube (PMT) which produces an electrical signal

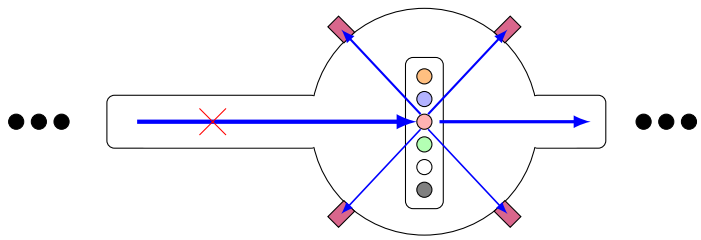

Figure 3: Concept of a thin foil Mott polarimeter. Here, a transversely polarized electron beam (shown in blue) is incident on a thin target. The polarization is shown in red. Upon scattering, an asymmetry can be seen in the detectors. This figure shows two detectors on each side. These detectors are placed at both the maximum and minimum of the Sherman function to help observe false asymmetries. The targets are then swapped and the process is repeated.

proportional to the initial optical signal. This process is shown in Fig. 4.

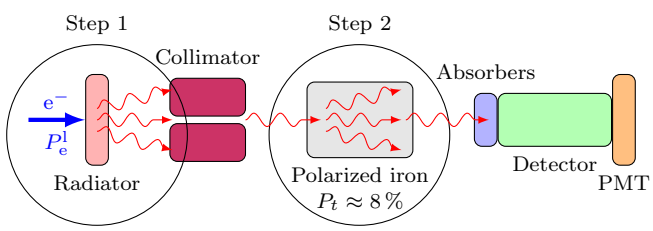

Figure 4: Concept of a Compton transmission polarimeter. Here, an incident electron beam carries a longitudinal polarization P_e^l, which produces circularly polarized bremsstrahlung photons upon striking a radiator. These photons are then collimated before a polarized iron target where the photons undergo polarized Compton scattering. Different electron beam helicities produce an asymmetry that can be observed in a subsequent detector consisting of a scintillating crystal and PMT. Once the analyzing power is calibrated, measuring the asymmetry provides a measurement of the beam polarization.

Observing an energy deposited asymmetry by experiment is not possible due to the large number of photons contributing to the detector signal causing the data rate to be too high to resolve individual events. Instead, the electrical signal is integrated over the entire time when the electron beam had the same helicity. This time period is known as a helicity window. Helicity windows are generated in an equal number within in a given cell. A cell can contain 2, 4, or even 8 helicity windows. The asymmetry is calculated for the case of 4 windows (known as a quartet) via

$$A_T^{\pm} = \frac{\pm(w_1 + w_4) \mp (w_2 + w_3)}{w_1 + w_2 + w_3 + w_4}, \tag{11}$$

where the $\pm$ corresponds to the helicity of the first window. Now, for a given run period where the asymmetry is desired, all the different A_T values for both helicity states are plotted in a histogram and the average is extracted. If the original beam polarization was well known, $\mathcal{A}_{\text{eff}}$ can be calibrated. When a new measurement needs to be made, the measured asymmetry and the effective analyzing power can be used to extract the polarization.

4 Measurements

4.1 Jefferson Lab Micro-Mott Polarimeter

The retarding field Mott polarimeter at Jefferson Lab, shown in Figure 5, created a low energy electron beam at -268 eV from bulk GaAs using 780 nm light. Light at 780 nm excites electrons close to the band gap which yields a theoretical maximum polarization of 50 %. This beam is guided electrostatically toward a gold target bias at +20 kV. This bias accelerated the electron beam to just over +20 keV where scattering occurred. The scattered electrons are then decelerated as they approach the detectors. In front of the detectors are the retarding field grids which are repulsively bias from -150 V to -320 V.

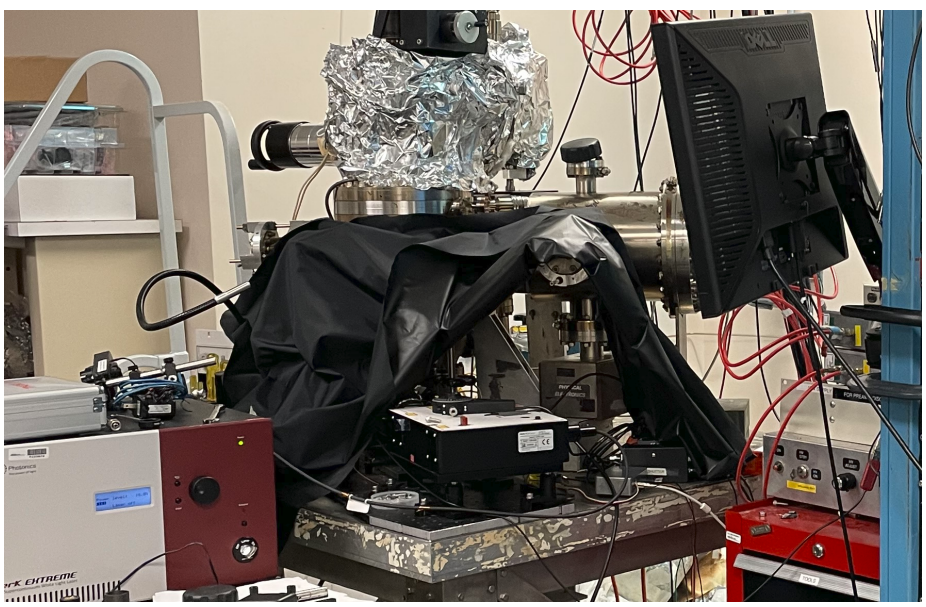

Figure 5: Picture of the Jefferson Lab Micro-Mott Polarimeter.

Figure 6 shows the asymmetry at each of these retarding field voltages where a linear fit has been applied to extract the asymmetry at -268 keV. Here, the asymmetry is 5.64 $\pm$ 0.27 % and the Sherman function at the scattering energy

at 20 keV is 20.1 % which yields a beam polarization of 28.06 ± 1.31 %. Bulk GaAs typically produces a beam with 25 to 40 % polarization; therefore, this result is well within expectations.

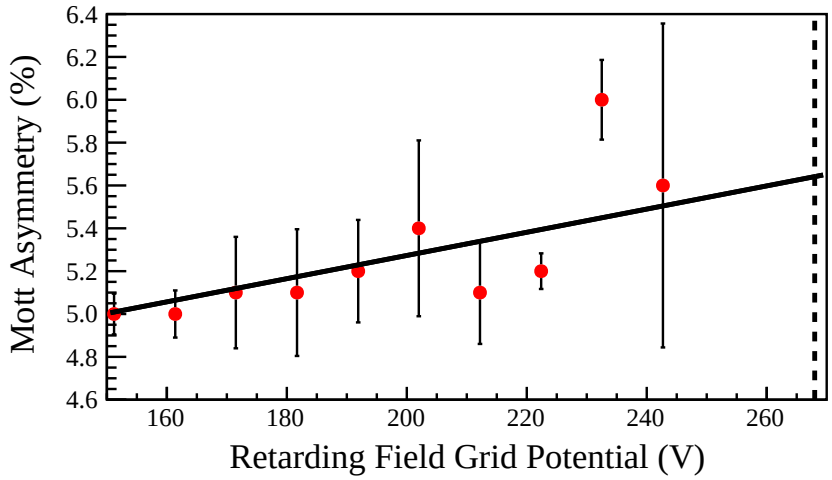

Figure 6: Asymmetry as a function of retarding field voltage in the Jefferson Lab Micro-Mott.

4.2 UITF keV Mott Polarimeter

The UITF thin foil Mott polarimeter (see Figure 7) operated using the extrapolation in Eq. 10. This polarimeter was optimized for operation at 100 keV where the detector angles correspond to the maximum magnitude of the Sherman function at 100 keV. However, this polarimeter has most recently been operated at 180 keV to study the polarization of a bulk GaAs photocathode (ultimately for calibration of the Compton transmission polarimeter). In this calibration 780 nm light was again used to excite electrons in the photocathode. The polarized electron beam is then directed incident on one of six target-ladder positions. Four of them are for gold foils (40 nm, 60 nm, 70 nm, and 80 nm thicknesses [25]), one is for a beam viewer, and one for a through-hole.

The asymmetry results of these four target thicknesses are shown in Figure 8. These asymmetries take advantage of both a Left-Right asymmetry as well as helicity reversal asymmetry to produce an asymmetry using the cross-ratio method [24]. Next, the zero-thickness extrapolation was applied to yield a zero-thickness asymmetry of (15.9 ± 0.4) % and a β of (0.0028 ± 0.0004)/nm. Together with the Sherman function at 120 degrees (location of the detectors) equal to 42.6 %, a beam polarization of (37.4 ± 0.8) % can be extracted. This

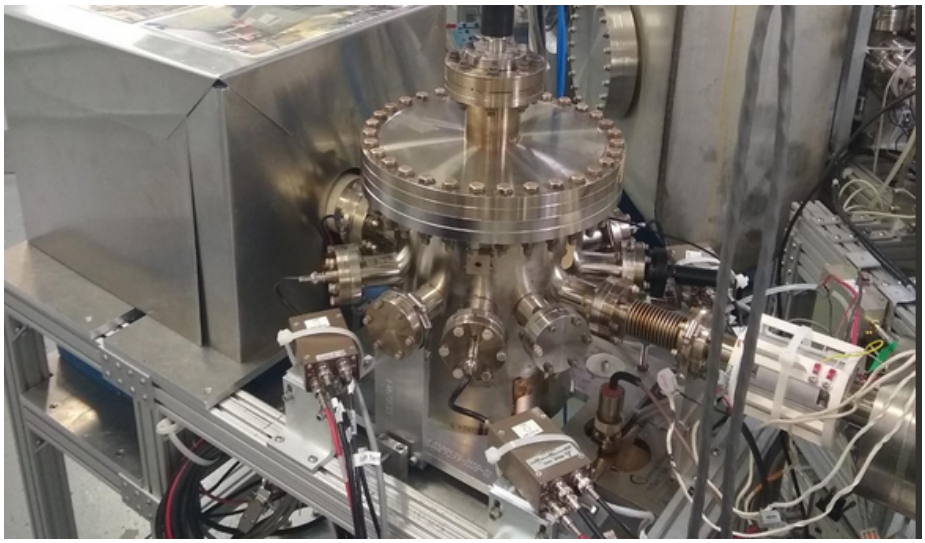

Figure 7: Picture of the UITF Mott polarimeter as installed.

polarization is well within expectations for bulk GaAs and is an excellent example of a thin foil Mott polarimeter.

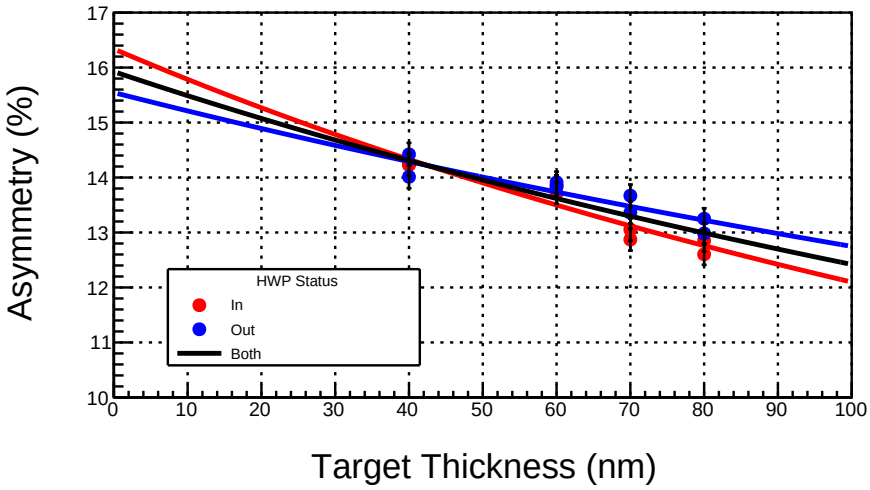

Figure 8: Asymmetry as a function of target thickness in the Jefferson Lab UITF Mott polarimeter. HWP status is used to reverse the helicity.

4.3 UITF Compton Transmission polarimeter

Calibration of the UITF Compton Transmission polarimeter (see Figure 9) required the beam polarization from the upstream Mott polarimeter given in the previous section (37.4 ± 0.8 %). At both 5 and 7 MeV, electron beams were sent incident on a 6 mm copper radiator. Next, the bremsstrahlung radiation was sent through a 14.6 cm long copper collimator with a bore of diameter of 0.8 cm. The remaining photons traveled through the polarized target which was a 7.5 cm long iron alloy solenoid magnet. The solenoid field was operated at ± 5 A to polarize electrons in the magnet core to produce the transmission asymmetry. The remain photons traveled through three 14 mm copper absorbers to reduce the photon count. Finally, photons that reached the detector deposited their energy in a scintillating crystal made of $Bi_4Ge_3O_{12}$ (BGO) which produced the optical signal for the PMT.

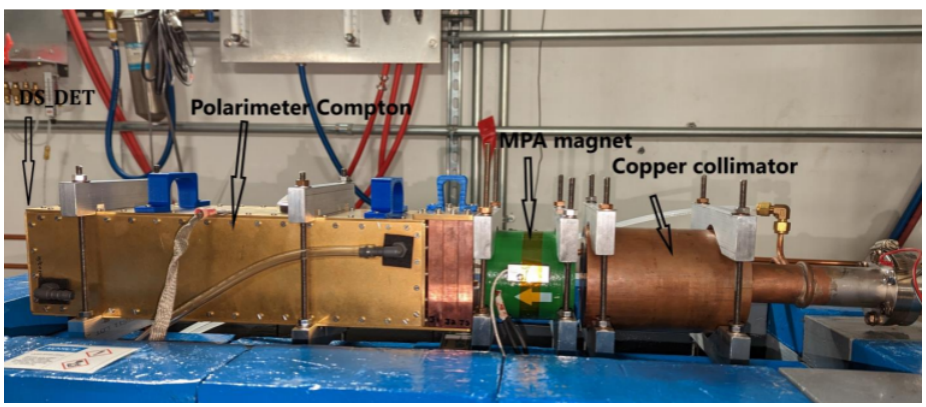

Figure 9: Picture of the UITF Compton Transmission polarimeter.

The helicity was generated in 4 window cells which were used to measure the transmission asymmetry. After optimizing beam current to 6 nA, a sequence of runs were taken and the asymmetry was observed in each run. An example of a run asymmetry is shown in Fig. 10.

The average of these runs is taken to be the asymmetry and was on the order of half a percent. The division of the asymmetry by the known beam polarization yields the calibrated effective analyzing power which can be used to extract beam polarization in future studies. The analyzing powers at 5 and 7 MeV are given in Equations 12 and 13.

$$\mathcal{A}_{\text{eff}}^{5\,\text{MeV}} = \frac{(0.452 \pm 0.004)\%}{(37.4 \pm 0.8)\%} = 1.20 \pm 0.03\% \tag{12}$$

$$\mathcal{A}_{\text{eff}}^{7\,\text{MeV}} = \frac{(0.481 \pm 0.007)\%}{(37.4 \pm 0.8)\%} = 1.29 \pm 0.04\% \tag{13}$$

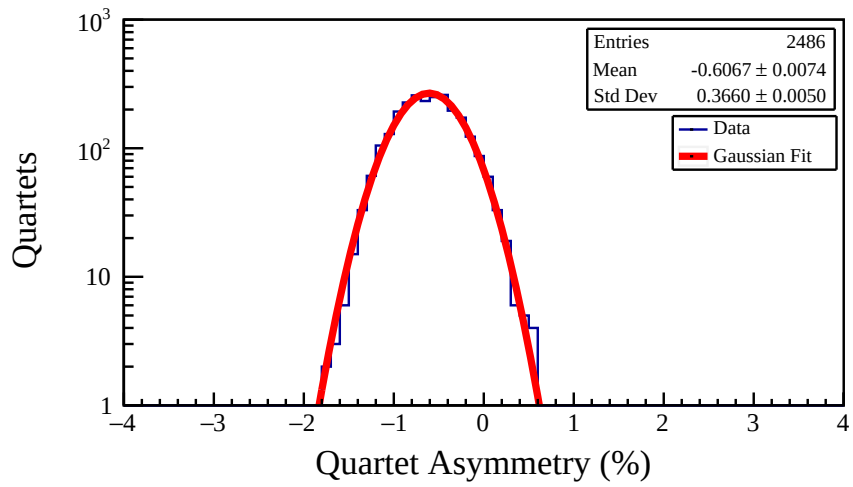

Figure 10: Compton transmission asymmetry for a chosen run during the calibration of the UITF Compton transmission polarimeter. The asymmetry is the mean of the histogram.

5 Comparison

When choosing a polarimeter, one must decide which method will encapsulate all the needs of the users. Different situations call for different polarimeters and it is up to a potential user to decide which technique best suits the experiment. Here, a comparison offering the attractions as well as potential drawbacks of each technique is given in Table 1.

Asymmetries are much higher in Mott-scattering polarimeters which leads to higher accuracy for the polarization in the same amount of measurement time. This is also the case for the analyzing power which means less time is required to make a measurement of equal accuracy. However, this larger asymmetry comes at the expense of requiring transverse polarization. GaAs based photocathodes produce longitudinal polarization so the spin must be rotated for Mott polarimetry to be useful. For the low energy retarding field polarimeters, this issue is circumvented using electrostatic bending which changes the momentum without altering the polarization, but higher energy thin foil polarimeters require spin manipulation techniques such as Wien filters [26] to rotate the spin transverse. This is not the case for Compton transmission polarimetry.

The available energy range may also effect the usefulness of a polarimeter. Retarding field polarimeters are limited by the bias applied to the target and thin foil polarimeters are restricted by the maximum of the Sherman function. At 10 MeV the maximum occurs at nearly 180 degrees, where the scattered elec-

	Retarding Field Mott	Thin Foil Mott	Compton Transmission
Effective Analyzing Power	20.1 % [8]	38.02 %* [17] 39.21 %† [24]	1.29 % [17]
Figure of Merit ($\%^2$ nA)	$\sim 10^2$	$\sim 10^3$ to 10^6	~ 10
Spin Direction	Transverse	Transverse	Longitudinal
Target Polarization	No	No	Yes
Beam Energy	<20keV	20keV<E<10MeV	1MeV<E<1000MeV
Beam Current	∼nA	$\sim \mu$A	∼nA
Detection	Primary (e^-)	Primary (e^-)	Secondary (γ)

Table 1: A table highlighting the key features of the three types of polarimeters discussed in this work. The statistical figure of merit can be found by multiplying the analyzing power squared by the average beam current. *For a target of thickness 40 nm at 180 keV. †For a target of thickness 1 µm at 5 MeV.

trons will interfere with the incident electron beam causing disruptions. Compton transmission polarimetery is not limited by scattering angle or target bias but by the energy required to produce and analyze the high energy photons (target thickness).

Furthermore, the maximum electron beam current depends on the energy chosen. For Mott-scattering the scattering cross-section decreases with beam energy. This decrease allows for higher currents at higher energies. Thin foil polarimeters can observe beam currents in the μA range if the beam energy is above an MeV while retarding field polarimeters are limited to nA due the much higher cross-section magnitude. Similarly, the Compton cross section is sensitive and is also limited to nA.

Finally, the geometry dependence may impact selection. Compton transmission polarimetry requires a target thickness that maximizes the asymmetry. For higher and higher energies, the target can quickly become extremely thick. Mott polarimetry requires placing the detectors to maximize the asymmetry which can be difficult depending on the energy selected, especially for higher energy. Clearly, all polarimeters have a purpose and it is on the user to select the correct instrument for their study.

6 Summary

Electron polarimetry is an important tool in the measurement of spin polarization of electron beams. At Jefferson Lab a number of polarimeters exist, each relying upon different physics (Mott, Møller, Compton) to extract the beam polarization. In this work we have discussed the operational principle behind three polarimeters at Jefferson Lab. Furthermore, we have shown experimental results measuring electron beam polarization using each of the three polarimeters. Finally, we offer a comparison between each technique weighing both pros and cons to highlight where each technique thrives.

References

[1] Christine A. Aidala, Steven D. Bass, Delia Hasch, and Gerhard K. Mallot. The spin structure of the nucleon. *Rev. Mod. Phys.*, 85:655–691, Apr 2013.

[2] Alexandre Deur, Stanley J Brodsky, and Guy F de Té ramond. The spin structure of the nucleon. *Reports on Progress in Physics*, 82(7):076201, jun 2019.

[3] Volker D. Burkert. Jefferson lab at 12 gev: The science program. *Annual Review of Nuclear and Particle Science*, 68(1):405–428, 2018.

[4] D.E. King, D.C. Jones, C. Gal, D. Gaskell, W. Henry, A.D. Kaplan, J. Napolitano, S. Park, K.D. Paschke, R. Pomatsalyuk, and P.A. Souder. Precision møller polarimetry for prex-2 and crex. *Nuclear Instruments and Methods in Physics Research Section A: Accelerators, Spectrometers, Detectors and Associated Equipment*, 1045:167506, 2023.

[5] A. V. Glamazdin, V. G. Gorbenko, L. G. Levchuk, R. I. Pomatsalyuk, A. L. Rubashkin, P. V. Sorokin, D. S. Dale, B. Doyle, T. Gorringe, W. Korsch, V. Zeps, J. P. Chen, E. Chudakov, S. Nanda, A. Saha, and A. Gasparian. Electron beam møller polarimeter at jlab hall a, 1999.

[6] T. Pussieux and Compton Polarimeter collaboration. Electron beam polarization with the Compton polarimeter at JLab. *AIP Conference Proceedings*, 570(1):761–764, 06 2001.

[7] N. F. Mott. The Scattering of Fast Electrons. *Proc. R. Soc. Lond*, 124:425–442, 1929.

[8] J.L. McCarter, M.L. Stutzman, K.W. Trantham, T.G. Anderson, A.M. Cook, and T.J. Gay. A low-voltage retarding-field mott polarimeter for photocathode characterization. *Nuclear Instruments and Methods in Physics Research Section A: Accelerators, Spectrometers, Detectors and Associated Equipment*, 618(1):30–36, 2010.

[9] D. Conti, S. Navert, K. Bodek, W. Haeberli, S. Kistryn, J. Lang, O. Naviliat, E. Reichert, J. Sromicki, M. Steigerwald, E. Stephan, and J. Zejma. Mott scattering of multi-MeV electrons from heavy nuclei. In *The Seventh International Workshop on polarized gas targets and polarized beams*, volume 421 of *American Institute of Physics Conference Series*, pages 326–335, January 1998.

[10] J. Sromicki, K. Bodek, D. Conti, St. Kistryn, J. Lang, S. Navert, O. Naviliat-Cuncic, E. Stephan, C. Sys, J. Zejma, W. Haeberli, E. Reichert, and M. Steigerwald. Polarization in mott scattering of multi-mev electrons from heavy nuclei. *Phys. Rev. Lett.*, 82:57–60, Jan 1999.

[11] T. Zwart, E. C. Booth, M. Farkhondeh, W. A. Franklin, E. Ihloff, J. L. Matthews, E. Tsentalovich, and W. Turchinetz. Transmission Polarimetry at MIT Bates. *AIP Conference Proceedings*, 675(1):1011–1015, 07 2003.

[12] Townsend Zwart, E. Booth, F. Casagrande, K. Dow, M. Farkhondeh, W. Franklin, E. Ihloff, K. Jacobs, J. Matthews, R. Milner, T. Smith, C. Tschalaer, E. Tsentalovich, W. Turchinetz, and F. Wang. Polarized electrons at Bates: Source to storage ring. *AIP Conference Proceedings*, 588(1):343–349, 09 2001.

[13] T. J. Gay and F. B. Dunning. Mott electron polarimetry. *Review of Scientific Instruments*, 63(2):1635–1651, 1992.

[14] Noah Sherman. Coulomb scattering of relativistic electrons by point nuclei. *Phys. Rev.*, 103:1601–1607, Sep 1956.

[15] Xavier Roca-Maza. personal communication.

[16] X. Roca-Maza. Theoretical calculations for precision polarimetry based on mott scattering. *Europhysics Letters*, 120(3):33002, feb 2018.

[17] G. Blume, M. Bruker, C. Cuevas, H. Dong, B. Fernandes Neres, P. Ghoshal, S. Gopinath, J. Grames, S. Gregory, G. Hays, C. Le Galliard, S. Marsillac, B. Moffit, T. Nguyen Trung, M. Poelker, R. Suleiman, E. Voutier, and S. Zhang. A compton transmission polarimeter for dc and srf electron photo-injectors. In preparation, 2023.

[18] Haakon Olsen and L. C. Maximon. Photon and Electron Polarization in High-Energy Bremsstrahlung and Pair Production with Screening. *Phys. Rev.*, 114:887–904, 1959.

[19] E. A. Kuraev, Yu. M. Bystritskiy, M. Shatnev, and E. Tomasi-Gustafsson. Bremsstrahlung and pair production processes at low energies, multi-differential cross section and polarization phenomena. *Phys. Rev. C*, 81:055208, 2010.

[20] E. Voutier, Th. S. Bauer, H. W. den Bok, M. E. Brandan, Z. Papandreou, and H. W. Willering. Analytical method for polarimeter design optimization. *Nucl. Instrum. Meth. A*, 430(1):110–126, 1999.

[21] S. Agostinelli et al. Geant4—a simulation toolkit. *Nucl. Instrum. Meth. A*, 506(3):250–303, 2003.

[22] J. Allison et al. Geant4 developments and applications. *IEEE T. Nucl. Sci.*, 53(1):270–278, 2006.

[23] J. Allison et al. Recent developments in geant4. *Nucl. Instrum. Meth. A*, 835:186–225, 2016.

[24] J. M. Grames, C. K. Sinclair, M. Poelker, X. Roca-Maza, M. L. Stutzman, R. Suleiman, Md. A. Mamun, M. McHugh, D. Moser, J. Hansknecht, B. Moffit, and T. J. Gay. High precision 5 mev mott polarimeter. *Phys. Rev. C*, 102:015501, Jul 2020.

[25] Lebow Company.

[26] G. G. Palacios Serrano, P. A. Adderley, J. M. Grames, C. Hernandez-Garcia, and M. Poelker. High-gradient wien spin rotators at jefferson lab. *NAPAC2022*, 9 2022.